AN AUTOMATIC MICROCALCIFICATION DETECTION SYSTEM BASED ON A HYBRID NEURAL NETWORK CLASSIFIER

A. Papadopoulos, D.I. Fotiadis and A. Likas

21 – 2001

Preprint, no 21 – 01 / 2001

Department of Computer Science
University of Ioannina
45110 Ioannina, Greece

An automatic microcalcification detection system based on a hybrid neural network classifier

A. Papadopoulos[1], D.I. Fotiadis[2] and A. Likas[2]

[1] Department of Medical Physics, Medical School

[2] Department of Computer Science

University of Ioannina,

GR 45110 Ioannina, Greece

Correspondence should be addressed to
Dr. D. I. Fotiadis
Department of Computer Science
University of Ioannina
45110 Ioannina, GREECE
Tel:+30 651 98803, fax: +30 651 98889
e-mail:fotiadis@cs.uoi.gr

Abstract:

A hybrid intelligent system is presented for the identification of microcalcification clusters in digital mammograms. The proposed method is based on a three step procedure: (a) preprocessing and segmentation, (b) regions of interest specification, and (c) feature extraction and classification. The reduction of false positive cases is performed using an intelligent system containing two sub-systems: a rule based and a neural network sub-system. In the first step of the classification schema 22 features are automatically computed which refer either to individual microcalcifications or to groups of them. Further reduction in the number of features is achieved through PCA analysis. The proposed methodology is tested using the Nijmegen and the MIAS mammographic databases. The detection specificity is 1.80 and 1.15 false positive clusters per image, for the Nijmegen and MIAS dataset respectively, at the sensitivity level higher than 0.90.

Key words:

Microcalcification detection, Hybrid neural network, CAD, Mammography,

1. Introduction

Breast cancer is currently one of the leading causes of death among women worldwide. Regular mammographic screening projects for women of certain age or high-risk groups is taking place in developed countries. Early detection is the key for improving breast cancer prognosis [35]. Mammography is the most effective procedure for detecting non-palpable cancers even when the size of the abnormality is minimal [33, 51]. One of the early signs of breast cancer is the presence of microcalcification clusters at the mammogram of asymptomatic women. However, a number of such findings could be missed or misinterpreted by doctors, due to the particularly small size and low contrast that they usually exhibit in an inhomogeneous mammographic background. Thus, the task of the radiologist is tedious in the case where a significant number of mammograms require fast and accurate interpretation. For this reason, a reliable automated computer-aided diagnosis system (CAD) could be very useful, providing a valuable "second opinion'' to a radiologist, especially to a non-expert one.

In the literature, several techniques have been proposed to detect the presence of microcalcifications using various methodologies. In what concerns image segmentation and specification of regions of interest (ROIs), several methods have been proposed such as classical image filtering and local thresholding [8, 11, 32, 36], techniques based on mathematical morphology [12, 49], stochastic fractal models [21, 22], wavelet analysis [2, 6, 18, 19, 37, 41, 45, 46] and multiscale analysis based on a specialized Gaussian [26]. In what concerns the characterization of regions of interest various classification methods have been reported suggested as rule-based systems [8, 11], fuzzy logic systems [10], statistical methods based on Markov random fields [16] and Support Vector Machines [2]. Nevertheless, the most work reported in the literature employs neural networks for cluster characterization [9, 23, 27, 30, 43, 44, 47, 50]. Typically, a neural network accepts as input features computed for a specific region of interest and provides as output a characterization of the region as true

microcalcification cluster or not. Recently, neural networks have also been used to characterize a microcalcification as malignant or benign [5, 20, 33, 39].

In this paper we present an intelligent system (Fig. 1) for the identification of microcalcification clusters in a digitized mammographic image. The system, as it is described in section 2, consists of three modules: the preprocessing and segmentation, the ROI specification and the feature extraction and the classification module. The latter is a hybrid classification schema composed of a rule based and a neural network sub-system. The proposed system is fast and accurate in the detection of ROIs. We employ an additional characteristic for ROI characterization that is related with the existence of a small ROI in the neighborhood of a large one. In addition, we have found that performance is improved in the case where PCA analysis is used to reduce the number of features. The method is fully automated and provides satisfactory results in two well – known datasets: the Nijmegen and the MIAS mammographic databases as it is described in section 3. It must be noted that the proposed hybrid system performs better compared with the case where either the rule-based or the neural network subsystem are solely employed for classification.

2. Material and methods

2.1 Image datasets

For the development and evaluation of the proposed method we use the Nijmegen [16] and the MIAS [38] databases. The first contains 40 mammograms of both craniocaudal and mediolateral oblique views from 21 patients. Digitization has been carried out using an Eikonix 1412 CCD camera with 0.1 mm pixel size and 12 bit grey depth. The size of each image is 2048×2048 pixels. For each image a lookup table is provided for conversion-rescaling from 12 to 8 bit format based on noise characteristics [16]. One or more microcalcification clusters are annotated in each mammogram by expert radiologists using a

circle enclosing the abnormality. The total number of annotated clusters in the database is 105. It must be noted that the Nijmegen dataset digitization characteristics are different from the MIAS dataset and we resampled the Nijmegen images to change the pixel size from 100 to 50 μm, because our software originally was developed to handle 50 μm images.

The second dataset contains 20 images and has been developed by the Mammographic Image Analysis Society (MIAS) [38]. Each mammographic image is obtained from the medio-lateral oblique view and is digitized with spatial resolution 50 μm and 8 bit grey depth. A circle enclosing the abnormality indicates each cluster area. The database contains a number of 25 annotated clusters.

The proposed system is implemented in three stages. The first is related to image segmentation, the second with the identification of candidate ROIs, and the third with the characterisation of each ROI as cluster of microcalcifications or not.

2.2 Preprocessing and Segmentation Module

In a typical mammogram several different areas are present such as the image background, the tissue area, and informative marks. At the beginning of preprocessing it is necessary to locate the breast region. For this reason we apply a skin-line segmentation procedure by setting equal to zero the image pixels with intensity less than 20 (for 0-255 grey levels). Most of those pixels belong to the background area, although a small number exists belonging to the tissue area close to the breast surface. This thresholding procedure results in a binary image of white objects on a black background. Neighbouring white pixels with connectivity of eight are grouped together to form objects corresponding either to the breast region or to marks and film artefacts. The largest object corresponds to the breast region (Fig. 2) and close to the breast outline a number of very small objects appear. These are actually part of the breast region but, due to thresholding, they appear as distinct objects. To deal with this

problem we apply morphological dilation with a structure element radius of 30 pixels (~1.5 mm). This results in an expansion of breast region outline, which includes all the nearby located objects. All the pixels that do not belong to the expanded breast area are set to zero, resulting in the removal of background, marks and artefacts. The artefacts located at the boundary of the breast region, at the chest side, forming a thick line are eliminated too. The minimum rectangle containing the breast region is automatically drawn and it is used in the subsequent processing stages.

At first, the mammogram is considered as a 3D plot with the third axis (z) corresponding to the intensity of each pixel (Fig. 3a). The whole image is split into 30×30 sub-regions and, using bicubic interpolation, a second plot is obtained representing the intensity level of the microcalcification local background (Fig. 3b). The interpolated image is subtracted from the original mammogram producing a third image with each pixel value providing the difference between the original and local background pixel values. The pixels with positive values are identified and a percentage of them (5 %) with the highest values is selected producing a binary image and also specifying a threshold value (the lowest value among the selected pixels). The reason for the above selection is that the objects of interest (microcalcifications) are characterized by higher intensity compared to their background. In a typical image, the number of selected pixels is quite large and in subsequent processing a fraction of them will be removed. If the amount of the selected pixels is lower than 10% of the total number of pixels of the cropped mammogram, the pixels with intensity higher than half of the previously specified threshold are added. In such a way an adequate number of pixels are included in the obtained binary image (A). This case occurs when the mammogram exhibits very low contrast usually due to erroneous exposure conditions.

Next a contrast enhancement filter is applied with 9×9 kernel having central element equal to 80 and all the other elements equal to –1 [31, 34]. 5% of the pixels having the highest

intensity are selected, producing a second binary image (B). The outcome of the segmentation module is an image produced by the logical summation (AND) of the two binary images A and B. It contains the pixels that have high intensity values and, at the same time, quite high intensity values in comparison with the background intensity of their local neighbourhood (Fig. 4).

2.3 Regions of interest specification

In the segmented image obtained in the previous stage, neighbouring pixels with connectivity of eight are grouped together to create possible microcalcification objects. Objects containing one or two pixels are rejected since they are considered as artefacts [9]. Since the diagnostic information is based on the existence of groups of objects, individual objects (possibly artefacts) should be removed. The elimination of these artefacts is achieved through the use of morphological operators. The application of the erosion operator (with structure element a 3×3 kernel of unit value) results in the removal of all objects apart from those that have at least one innermost pixel that is not part of its boundary. In this way only inner pixels that belong to large objects remain. These pixels correspond to the centres of ROIs, which are generated using the dilation operator with a 3×3 structure element of unit value. The dilation is repeated 50 times in order to produce a ROI with sufficient area around the object.

The smallest possible size of ROI is 101×101 pixels and appears when the central pixel of an object is isolated and no other central pixel is located at a distance smaller than 100 pixels (which is the maximum allowed distance in order for two distinct objects to belong in the same ROI). This selection takes into account the mean distance among microcalcifications in a cluster [3]. A ROI that is not of minimum size is considered as having been generated from a group of objects located in the same neighbourhood. In such case, two or more ROIs will be combined and a new enlarged ROI will be generated containing more than two of the original

objects. Based on the above methodology, several ROIs are identified in the mammogram and each of them is a candidate for being a true cluster of microcalcifications.

The set of ROIs is partitioned in two groups depending on their area. The first group contains those ROIs with area lower than 20,000 pixels (2×100×100), which is a reliable threshold value discriminating ROIs that are generated from individual objects. The second group contains the remaining ROIs which contain at least two nearby objects. This discrimination of ROIs defines a novel feature that will be used at the classification stage.

The existence of an individual object close to a ROI might be a problem in some cases. To resolve it a second dilation process is applied on the previous image, but only to the set of larger ROIs, using a 3×3 structure element in a 50-cycle repeated procedure. The resulting image contains usually one or two ROIs that include at least one large ROI and perhaps some small ROIs (of the previous image) that are close to the large one.

The above procedure constitutes an attempt to identify groups of objects that are candidate microcalcification clusters. The medical rule for the existence of microcalcification cluster is the presence of more than three microcalcifications in 1 cm^2 area [17]. Since this rule can be used for the reduction of false positive detected ROIs, all the regions that include less than two objects are eliminated. Using the above morphological analysis, a number of ROIs is specified.

2.4 Classification Module

The objective of the classification module is to categorize the specified ROIs as true microcalcification clusters or not. The large number of false positive clusters that are identified by the segmentation process makes the characterization task difficult. In order to specify the features that will be used as inputs to the classification system, at first 54 features

are identified and computed characterizing either an individual microcalcification (object) or a group of them in a specific ROI. Those features fall into three categories related with the intensity, shape and texture properties of each object. The group features are computed as the mean value of the five larger objects included in a ROI. The selection of the five larger microcalcifications is made since a very small microcalcification does not have enough pixels for reliable feature value computation [3].

An important feature that contributes significantly to the classification ability of the proposed system is whether a given ROI lies in the same neighbourhood with a larger ROI. Despite the fact that this feature is not related with some established medical rule, the discrimination performance of this feature is high. The last is a consequence of the way that the ROIs are generated. The existence of a small ROI near a large one introduces increased possibility for it either to be a true cluster or part of the large one. In any case, the inclusion of this feature increases the detection performance of the system.

Since the number of the computed features is quite large and their discriminative power varies, a feature validation together with feature selection procedure is applied. The receiver operating characteristic (ROC) curve is plotted for each feature and the area A_z under the ROC curve is computed. Features with the highest A_z are selected, resulting in a set of 22 features (Table 1). It must be noted that most of the selected features correspond to the mammographic characteristics that expert radiologists examine during a diagnostic procedure [42].

In the next step of the classification module the selected features are fed into a hybrid intelligent classification system, which consists of two components (Fig. 5): a rule based and a neural network component. We make the assumption that each rule of the rule based sub –

system employs at most two features. Therefore it is straightforward to visualise the data and identify the corresponding threshold values.

In the Nijmegen database the rule based sub-system contains three rules employing a single feature and one rule with two features. The employed features are the standard deviation of the microcalcifications' intensity in a cluster, the mean eccentricity value in a cluster, the entropy of a cluster and the standard deviation of the distances of microcalcifications from the cluster centre and the average microcalcifications' area in a cluster. All the rules, other than the cluster entropy, contribute to the removal of false positive clusters.

In the MIAS database four rules have been obtained each one employing one feature. The features with the higher discriminative capability are the area of a cluster, the average background intensity in each cluster, the highest entropy value of the clusters in each image (relative entropy value) and the existence of large area clusters in the neighbourhood of a cluster. All the features, apart from the second one, contribute to the classification of abnormal cases. It must be noted that the cluster entropy is a common feature in both datasets, something that underlines the importance of this particular feature.

All the ROIs characterized by the rule based sub-system are removed from the dataset. The remaining ROIs constitute the dataset (with 22 features per ROI) that will be used for construction of the neural network.

The neural network (Fig. 6) that is used for ROI characterisation is a feedforward neural network with sigmoid hidden nodes (Multiplayer Perceptron – MLP). In order to select an appropriate architecture (number of hidden layers and hidden nodes per layer) several networks were tested with one or two hidden layers and different number of hidden nodes. In order to reduce the dimensionality of the input vector, a principal components analysis (PCA) was applied to eliminate the features that contribute less than 3% to the total variation of the

data set. The PCA procedure transforms each 22-dimensional feature vector into a 9-dimensional feature vector that will constitute the input to the neural network. The components of each new feature vector are normalized to zero mean and unit variance.

Several training algorithms were implemented and tested: gradient descent methods, resilient backpropagation, conjugate gradient methods, and quasi Newton methods. The best results are obtained using a Quasi-Newton method, and more specifically, the one step secant - OSS algorithm [1].

To assess the performance of several architectures and training algorithms the two-fold cross validation method was employed. According to this procedure, the dataset is randomly divided into two subsets where the number of positive and negative cases in each subset is approximately equal. In a first experiment the training set corresponds to the first subset and the test set to the second one. In a second experiment the first subset corresponds to the test set and the second to the training set. The performance is calculated as the average test set performance in the two experiments.

To train a neural network we assume that positive (true) ROIs correspond to unit output while negative ones to zero output. Training is terminated either when the training error is less than a very small given value (10^{-5}) or when 2000 iterations have been performed.

During testing a threshold value is needed to classify an input case as true or false cluster based on the output value which ranges from zero to one. As the threshold value decreases from one to zero, a larger number of true positive cases is correctly characterised with an obvious increase of false positive cases. The network performance is measured using the area A_z under a ROC curve generated by plotting the true positive fraction (sensitivity) against the false positive fraction (specificity) of the cases for various threshold values. Alternatively, the

FROC curve may be used which considers the number of false positive clusters per image instead of the specificity value [7].

The finally selected network (the one with the best cross-validation performance) for the Nijmegen database has an input layer with nine nodes, two hidden layers with 20 and 10 sigmoid nodes respectively, and an output layer with one sigmoid node. For the MIAS database, the same neural network has also been used.

3. Results

Nijmegen Database

The segmentation process results in 446 candidate ROIs from which 115 are true. The difference is due to the fact that our system in some cases identifies two or more ROIs contained in a single annotated ROI. Using the rule based sub-system 215 ROIs are classified. Most of them are normal ROIs corresponding to artefacts and blood vessel type objects. 41 ROIs are true positive (TP), 167 are true negative (TN), 5 are false positive (FP) and 2 are false negative (FN) cases. Using the rule based sub-system 48% of the cases are characterised corresponding to 39 % of abnormal and 49 % of normal cases.

The performance of the hybrid system using two – fold cross-validation at the sensitivity level 0.90 is 1.8 false positive clusters per image. The use of the neural network results in 54 TP, 89 TN, 9 FN and 70 FP cases and the hybrid system results in 95 TP, 256 TN, 11 FN and 75 FP cases. The A_z area under the ROC curve is 0.912 (Fig. 7). The performance is high for a wide range of sensitivity. At the sensitivity level 0.79, the specificity is 0.86 (or 1.15 false positive clusters per image) and at the sensitivity level 0.96 the number of false positive clusters per image is 3.28 (Table 2).

It is also common in the related literature to report performance results where the complete dataset (including both the training and the test set) is used as a test set (for measuring the performance of the method), due to the limited number of available cases. In such case, as expected, the system performance is greatly improved. More specifically, at the specificity level of 1.18 false positive clusters per image, the sensitivity value obtained is 0.96 (Table 3). The area A_z is equal to 0.956 (Fig. 8).

In order to assess the performance benefits from the use of the hybrid system, we have conducted experiments to compare the method against the case where a single neural network is used a classification component instead of the hybrid system. More specifically the same network architecture was used but the rule based component was left out. The performance of this system at a sensitivity level of 0.90 was 4.25 false positive clusters per image (Table 4). The A_z area under ROC curve area is 0.825 (Fig. 9). Obviously these results are much worse than those obtained with the proposed hybrid classification system.

The MIAS Database

The MIAS database contains 20 digitised films that include microcalcification clusters. The total number of annotated clusters is 25. The segmentation process results in 193 candidate ROIs from which 34 are true. The rule based sub-system characterises 116 ROIs corresponding to 25 TP, 79 TN, 12 FP, and zero FN cases. The percentage of ROIs classified by the rule based sub-system is 73% of the abnormal and 50% of the normal cases.

The performance of the hybrid system using two–fold cross-validation at the sensitivity level 0.91 is 1.15 false positive clusters per image. The use of neural network at the remaining cases results in 4 TP, 57 TN, 3 FN and 11 FP cases and the entire hybrid system results in 29 TP, 136 TN, 3 FN and 23 FP cases. The A_z area under the ROC curve is 0.921 (Fig. 10). At sensitivity level 0.84, the specificity value is 0.90 (or 0.8 false positive clusters per image)

and at the sensitivity level 0.94 the specificity is 2.70 false positive clusters per image (Table 5).

If the performance of the hybrid neural network is measured in the complete data set (training and testing) the sensitivity improves to 0.94 at the specificity level of 0.92 or 0.65 false positive clusters per image (Table 6). The area A_z in this case is 0.968 (Fig.11). When a single neural network is solely used instead of the hybrid system, the performance deteriorates significantly: at sensitivity level 0.91, the specificity is 3.0 false positive clusters per image (Table 7). The A_z area under ROC curve is 0.866 (Fig. 12).

4. Discussion

The proposed system exhibits high performance in the detection of microcalcification clusters since it is able to identify more that 90% of the total number of clusters with a rather small number of false positive findings. The utilization of a hybrid intelligent classification component improves the performance of the system. A reduction of the false positive clusters cases is achieved without any cost for the sensitivity of the system. The absence of user adjustable parameters in the segmentation process ensures that it is straight forward to apply the method to other mammographic datasets.

Several techniques have been reported in the literature for the detection of microcalcification clusters using various methodologies. The performance of the proposed method is comparable with the reported results. For the Nijmegen dataset, Meersman et al. [24] using a neural network approach reported sensitivity level 0.84 and 2 false positive clusters per image. Using an adaptive filtering method Gurgan [15] achieved sensitivity one with 2.3 false clusters per image. Yu [47] obtained sensitivity 0.9 with 0.5 false clusters per image and Bazzani [2] obtained sensitivity 0.94 with 0.6 false clusters per image using an evaluation procedure that

incorporates the training set. Netsch [26] reported sensitivity 0.84 with 1 false positive cluster per image. Kassemeijer [16] obtained sensitivity 0.90 with 0.8 false positive clusters per image using an extended Nijmegen dataset (containing 25 additional images).

For the MIAS dataset, Diahi et al. [13] proposed a neural network system that is fed with predefined ROIs providing detection performance 0.95 for the whole dataset. Norhayati et al. [28], using triple-ring filter analysis, reported sensitivity 0.96 with 1.8 false positive clusters per image using an extended dataset containing 24 additional images without findings.

Concerning our methodology several comments can be made. First, the cluster detection procedure is greatly accelerated. Instead of using sliding windows and applying a medical rule in each of them (as happens in several other systems), our methodology detects the center of each ROI and then a window is drawn around it. Therefore, search for clusters based on the application of the medical rule is performed for a limited number of windows. In addition, ROIs are detected more accurately including a larger number of microcalcifications, which are consisted of more pixels.

At the feature extraction step 54 features are initially computed. Some of them are extracted from individual microcalcifications and others (group features) are the average values of the microcalcification cluster features. 22 features are kept after ROC analysis for each feature. Most of these features are also taken into account by medical experts during the visual mammogram interpretation. In addition, we introduce a new significant feature related with the existence of large ROIs in the neighborhood of a given ROI. The employed number of features is further reduced using PCA whose threshold has been experimentally specified. The use of PCA in conjuction with the hybrid intelligent system constitutes a novel characteristic of the method.

The proposed method detects microcalcification clusters in digitized mammograms eliminating the false groups of objects having similarities with the true clusters. In both datasets the performance of our method is high for a large range of sensitivities. This is an indication of robustness giving expectations for satisfactory performance using other datasets. It must be noted that the method performs well despite the fact that no processing for identification of line structures is included. The latter constitutes a natural direction for further enhancement of our method performance.

Additional patient features other than those obtained from the image such as family history, age, etc. might be included to improve the diagnostic value of our system. The next step of our work is to use hybrid systems to perform classification of identified clusters as malignant or not.

5. Conclusions

A hybrid intelligent system has been developed for the identification of microcalcification clusters in digitised mammograms. The method employs two components: a rule based and a neural network sub-system. We tested our system in the Nijmegen and the MIAS mammographic databases with satisfactory results. The achieved classification specificity is 1.80 and 1.15 false positive clusters per image, for the Nijmegen and MIAS dataset, respectively, at the sensitivity level of about 0.91.

Although the achieved performance is satisfactory further studies should be done in the elimination of falsely detected objects with line structure that are in most cases non-microcalcification items. Further testing has to be performed concerning the use of other databases as well as of original mammograms obtained from the clinical routine of the collaborating hospitals or screening population projects. Finally, future work will also be

directed towards the construction of a classification system that will perform discrimination between benign and malignant microcalcification clusters.

Acknowledgements

The present work is partially supported by the Greek General Secretariat of Research and Technology as part of the project "EPET II – PENED: Analysis and Design of Classification Methods for Computerized-Aided Detection of Breast Cancer from Radiological Data".
The Nijmegen database was provided by courtesy of the National Expert and Training Centre for Breast Cancer Screening and the Department of Radiology at the University of Nijmegen, the Netherlands.

References

[1] R. Battiti, First and second order methods for learning: Between steepest descent and Newton's method, *Neural Computation* 4(2) (1992) 141-166.

[2] A. Bazzani, A. Bevilacqua, D. Bollini, R. Brancaccio, R. Campanini , N. Lanconelli, A. Riccardi, D. Romani, G. Zamboni, Automated detection of clustered microcalcifications in digital mammograms using an SVM classifier, *European Symposium on Artificial Neural Networks* (2000) 195-200.

[3] D. Betal, N. Roberts, G.H. Whitehouse, Segmentation and numeral analysis of microcalcifications on mammograms using mathematical morphology, *Br J Radiol.,* 70(9) (1997) 903-917.

[4] C.M. Bishop, *Neural Networks for Pattern Recognition*, (Oxford University Press, Clarendon Oxford, 1996).

[5] M.J. Bottema, J.P. Slavotinek, Detection and classification of lobular and DCIS (small cell) microcalcifications in digital mammograms, *Pattern Recognition Letters* 21 (2000) 1209-1214.

[6] D. Brzakovic, P. Brzakovic, M. Neskovic, An approach to automated screening of mammograms, *SPIE Biomed. Image Processing. Biomed. Visual*. 2167 (1993) 868-886.

[7] D.P. Chakraborty, L.H. Winter, Free response methodology: Alternate analysis and a new observer-performance experiment, Radiol. 174(3) (1990) 873-881.

[8] H.P. Chan, K. Doi, S. Galhotra, C.J. Vyborny, H. MacMahon, P.M. Jokich, Image feature analysis and computer aided diagnosis in digital radiography: 1. Automated detection of microcalcifications in mammography, *Med. Phys*. 14 (1987) 538-548.

[9] H.P. Chan, S.C.B. Lo, B. Sahiner, K.L. Lam, M.A. Helvie, Computer-aided detection of mammographic microcalcifications: Pattern recognition with an artificial neural network, *Med. Phys*. 22(10) (1995) 1555-1567.

[10] H. Cheng, Y.M. Lui, R.I. Feiimanis, A novel approach to microcalcification detection using fuzzy logic techniques, *IEEE Trans. Med. Imag.* 17(6) (1998) 442-450.

[11] D.H. Davies, D.R. Dance, Automated computer detection of clustered calcifications in digital mammograms, *Phys. Med. and Biol.* 35(8) (1990) 1111-1118.

[12] J. Dengler, S. Behrens, J.F. Desage, Segmentation of microcalcifications in mammograms, *IEEE Trans. Med. Imag.* 12 (1993) 634-642.

[13] J.G. Diahi, C. Frouge, A. Giron, B. Fertil, Artificial neural networks for detection of breast cancer in mammography, *3rd Inter. Workshop on Digital Mammography* (1996) 329-334.

[14] R.C. Gonzalez, R.E. Woods, *Digital Image Processing* (Reading MA: Addison-Wesley 1993).

[15] M.N. Gurgan, Y. Yardimci, A.E. Cetin, Microcalcification detection using adaptive filtering and gaussianity tests, *4th Inter. Workshop on Digital Mammography* (1998)157-164.

[16] N. Karssemeijer, Adaptive noise equalization and recognition of microcalcifications in mammography, *Inter. J. Pattern Recog. Artif. Intel.* 7 (1993) 1357-1376.

[17] D.B. Kopans, *Breast Imaging.* (J.B. Lippincott, Philadelphia, 1989).

[18] M.J. Lado, P.G. Tahoces, A.J. Mendez, M. Souto, J.J. Vidal, A wavelet-based algorithm for detecting clustered microcalcifications in digital mammograms, *Med. Phys.* 26(7) (1999) 1294-1305.

[19] A.F. Laine, S. Schuler, J. Fan, W. Huda, Mamographic feature enhancement by multiscale analysis, *IEEE Trans. Med Imag.* 1905 (1994) 725-738.

[20] S.K. Lee, C.S. Lo, C.M. Wang, P.C. Chung, C.I. Chang, C.W. Yang, P.C. Hsu, A computer-aided design mammography screening system for detection and classification of microcalcifications, *Int. J. Med. Informt.* 60 (2000) 29-57.

[21] F. Lefebvre, H. Benali, R. Gilles, E. Kahn, R. Di Paola, A fractal approach to the segmentation of microcalcifications in digital mammograms, *Med. Phys*. 22 (4) (1995) 381-390.

[22] H. Li, K.J.R. Liu, S.C.B. Lo, Fractal modelling and segmentation for the enhancement of microcalcifications in digital mammograms, *IEEE Trans. Med. Imag.* 16 (6) (1997) 785-798.

[23] S.C. Lo, H.P. Chan, J.S. Lin, H. Li, M.T. Freedman, S.K. Mun, Artificial convolution neural network for medical image pattern recognition, *Neural Networks* 8(7/8) (1995) 1201-1214.

[24] D. Meersman, P. Scheunders, D. Van Dyck, Detection of microcalcifications using neural networks, *3rd Inter. Workshop on Digital Mammography* (1996) 287-290.

[25] C.E. Metz, ROC methodology in radiologic imaging, *Invest. Radiol*. 21(9) (1986) 720-733.

[26] T. Netsch, H.O. Peitgen, Scale-space signatures for the detection of clustered microcalcifications in digital mammograms, *IEEE Trans. Med. Imag*. 18(9) (1999) 774-786.

[27] R.H. Nigel, R.M. Nishikawa, J. Papaioannou, K. Doi, Analysis of methods for reducing false positives in the automated detection of clustered microcalcifications in mammograms, *Med. Phys*.25(8) (1998) 1502-1506.

[28] I. Norhayati, F. Hiroshi, H. Takeshi, E. Tokiko, Automated detection of clustered microcalcifications on mammograms: CAD system application to MIAS database, *Phys. Med. Biol.* 42 (1997) 2577-2589.

[29] A. Papadopoulos, D.I. Fotiadis, A. Likas, A hybrid neural method for microcalcification cluster detection in mammography, *Proc. of 4th Inter. Conf. on Neural Networks and Expert Systems in Medicine and Healthcare* (2001) 90-96.

[30] E.A. Patrick, M. Moskowitz, V.T. Mansukhani, E.I. Gruenstein, Expert learning system network for diagnosis of breast calcifications, *Invest. Radiol.* 26 (1991) 534-539.

[31] W.K. Pratt, *Digital Image Processing (*A Wiley-Interscience Publication, 1991).

[32] W. Qian, L.P. Clarke, M. Kallergi, H. Li, R. Velthuizen, R.A. Clark, M.L. Silbiger, Tree-structured nonlinear filter and wavelet transform for microcalcification segmentation in mammography, *SPIE Biomed. Image Processing and Biomed. Visual.* 12(4) (1993) 634-642.

[33] R.A. Schmidt, R.M. Nishikawa, Digital screening mammography. *Principles and Practice Oncol.,* 8 (1994) 1-16.

[34] F. Schmidt, E. Sorantin, C. Szepesvari, E. Graif, M. Becker, H. Mayer, K. Hartwagner, An automatic method for the identification and interpretation of clustered microcalcifications in mammograms, *Phys. Med. Biol.* 44 (1999) 1231-1243.

[35] R.A. Smith, Epidemiology of breast cancer categorical course in physics, Tech. Aspects Breast Imaging, *Radiol. Soc. N. Amer.* (1993) 21-33.

[36] T. Soni, J.R. Zeidler, W.H. Ku, Performance evaluation of 2-D adaptive prediction filters for detection of small objects in image data, *IEEE Trans. Image Processing* 2(3) (1993) 327-339.

[37] R.N. Strickland, H.I. Hahn, Wavelet transforms for detecting microcalcifications in mammography, *IEEE Trans. Med.Imag.* 15(2) (1996) 218-228.

[38] J. Suckling, J. Parker, D. Dance , S. Astley, I. Hutt, C. Boggis, I. Ricketts, D. Stamatakis, N. Cerneaz, S. Kok, P. Taylor, D. Betal, J. Savage, The mammographic images analysis society digital mammogram database, Exerpta Medica 1069 (1994) 375-378.

[39] W. Veldkamp, N. Karssemeijer, J.D.M. Otten, J.H.C.L. Hendriks, Automated classification of clustered microcalcifications into malignant and benign, *Med. Phys.* 27(11) (2000) 2600-2608.

[40] W. Veldkamp, N. Karssemeijer, Automated classification of clustered microcalcifications in digital mammograms: applications of artificial neural networks. Digital mammography, *Exerpta Medica* (1996) 23-30.

[41] T.C. Wang, N.B. Karayiannis, Detection of microcalcifications in digital mammograms using wavelets, *IEEE Trans. Med. Imag.* 17(4) (1998) 498-509.

[42] P. Whatmough, A.G. Gale, A.R.M. Wilson, Do radiologists agree on the importance of mammographic features?, *3rd Inter. Workshop on Digital Mammography* (1996) 111-116.

[43] Y. Wu, K. Doi, M.L. Giger, R.M. Nishikawa, Computerized detection of clustered microcalcifications in digital mammograms: application of artificial neural networks, *Med. Phys*. 19(3) (1992) 555-560.

[44] Y. Wu, M.L. Giger, K. Doi, C.J. Vyborny, R.A. Schmidt, C.E. Metz, Artificial neural networks in mammography: application to decision making in the diagnosis of breast cancer, *Radiol.* 187 (1993) 81-87.

[45] H. Yoshida, K. Doi, R.M. Nishikawa, Automated detection of clustered microcalcifications in digital mammograms using wavelet transform techniques, *SPIE Image Processing* 2167 (1994) 868-886.

[46] H. Yoshida, K. Doi, R.M. Nishikawa, M.L. Giger, R.A. Schmidt, An improved CAD scheme using wavelet transform for detection of clustered microcalcifications in digital mammograms, *Acad. Radiol*. 3 (1996) 621-627.

[47] S. Yu, L. Guan, A CAD system for the automated detection of clustered microcalcifications in digitised mammogram films, *IEEE Trans. Med. Imag*. 19(2) (2000) 115-126.

[48] W. Zhang, K. Doi, M.L. Giger, Y. Wu, M. Nishikawa, R.A. Schmidt, Computerized detection of clustered microcalcification in digital mammograms using a shift-invariant artificial neural network, *Med. Phys*. 19 (1994) 555-560.

[49] D. Zhao, Rule-based morphological feature extraction of microcalcifications in mammograms, *SPIE Med. Imag.* 1095 (1993) 702-715.

[50] B. Zheng, W. Qain, L.P. Clarke, Digital mammography: Mixed feature neural network with spectral entropy decision for detection of microcalcifications, *IEEE Trans. Med. Imag.* 15(5) (1996) 589-597.

[51] H.C. Zuckerman, The role of mammography in the diagnosis of breast cancer, in: Ariel IM, Cleary JB, eds., *Breast Cancer, Diagnosis and Treatment* (McGraw-Hill, New York, 1987) 152-172.

Table 1: Main features for cluster categorization.

Microcalcification (MC) cluster classification features	**Radiologists characterization features**
Number of MCs in cluster	Cluster elements (separable / countable)
Cluster area	Cluster size
Mean MC area	MCs size
STD of MCs area	Shape of elements within cluster
Mean MC compactness	Shape of elements within cluster
Mean MC elongation	Shape of elements within cluster
STD of MC elongation	Shape of elements within cluster
STD of MC intensity	Density of calcifications
Mean MC background intensity	Density of calcifications
Mean contrast	Contrast of calcifications
Cluster eccentricity	Shape of cluster
Mean distance from cluster centroid	Calcification distribution
Neighbouring with a larger cluster	Cluster distribution
Cluster Entropy	Calcification's distribution
Spreading of MCs in cluster	Calcification's distribution
Cluster elongation	Cluster's shape
Mean local MC background	Density of calcifications
Mean MCs intensity	Density of calcifications
STD of MC compactness	Shape of elements within cluster
STD of distances from cluster centroid	Calcification's distribution
Area of the cluster convex hull	Shape of cluster
The length of the cluster convex hull	Shape of cluster

Table 2: Performance of the proposed hybrid intelligent system tested for the Nijmegen dataset (cross validation).

Sensitivity	Specificity	False positive clusters / image
0.79	0.86	1.15
0.84	0.82	1.45
0.90	0.77	1.80
0.96	0.60	3.28

Table 3: Performance of the proposed hybrid intelligent system tested for the Nijmegen dataset (complete set).

Sensitivity	Specificity	False positive clusters / image
0.89	0.92	0.68
0.93	0.89	0.95
0.96	0.86	1.18

Table 4: Performance of the neural network system without rules employment, tested for the Nijmegen dataset (cross validation).

Sensitivity	Specificity	False positive clusters / image
0.83	0.68	2.70
0.90	0.49	4.25
0.96	0.36	5.90

Table 5: Performance of the proposed hybrid intelligent system tested for the MIAS dataset (cross validation).

Sensitivity	Specificity	False positive clusters / image
0.84	0.90	0.80
0.91	0.86	1.15
0.94	0.66	2.70
0.97	0.55	3.55

Table 6: Performance of the proposed hybrid intelligent system tested for the MIAS dataset (complete set).

Sensitivity	Specificity	False positive clusters / image
0.91	0.92	0.65
0.94	0.92	0.65
0.97	0.88	0.95

Table 7: Performance of the neural network system without rules employment, tested for the MIAS dataset (cross validation).

Sensitivity	Specificity	False positive clusters / image
0.82	0.68	2.50
0.91	0.62	3.00
0.97	0.58	3.30

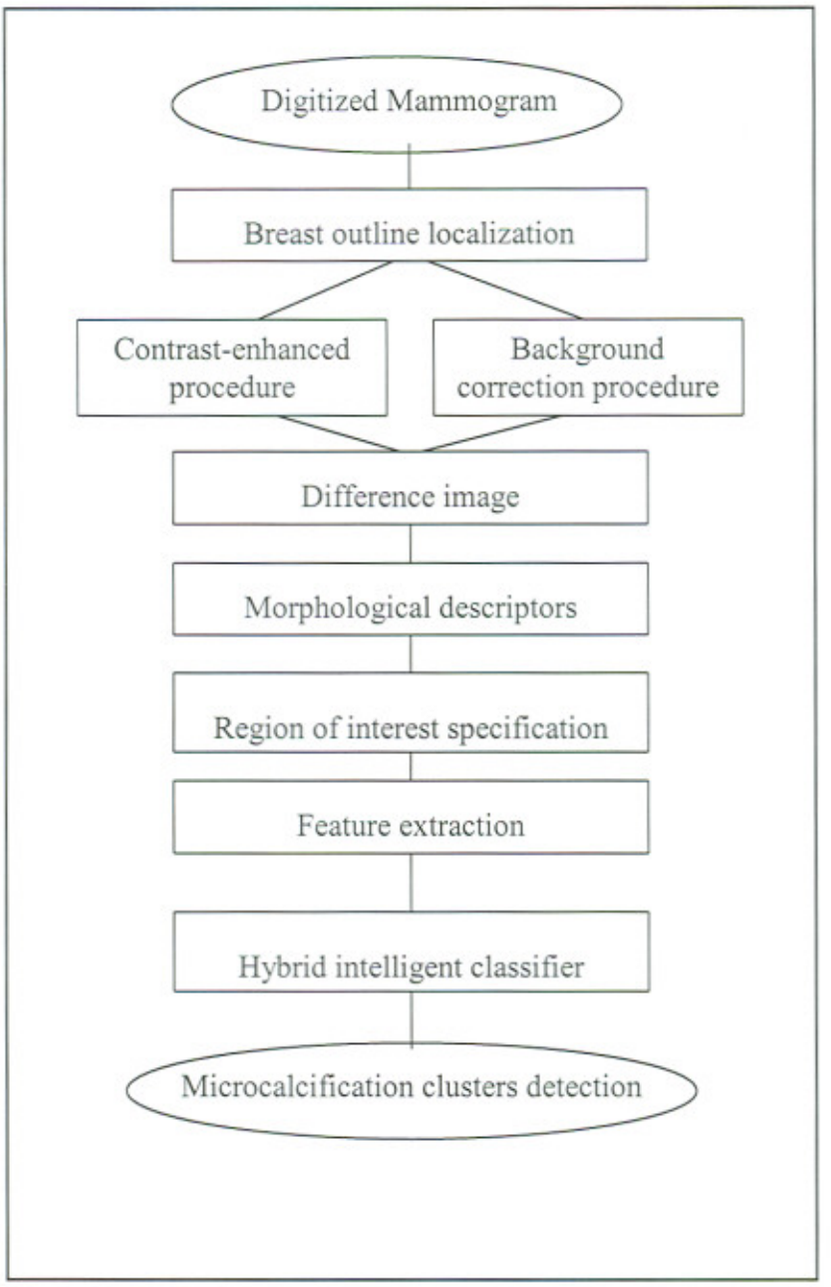
Digitized Mammogram
Breast outline localization
Contrast-enhanced procedure
Background correction procedure
Difference image
Morphological descriptors
Region of interest specification
Feature extraction
Hybrid intelligent classifier
Microcalcification clusters detection

Fig.1

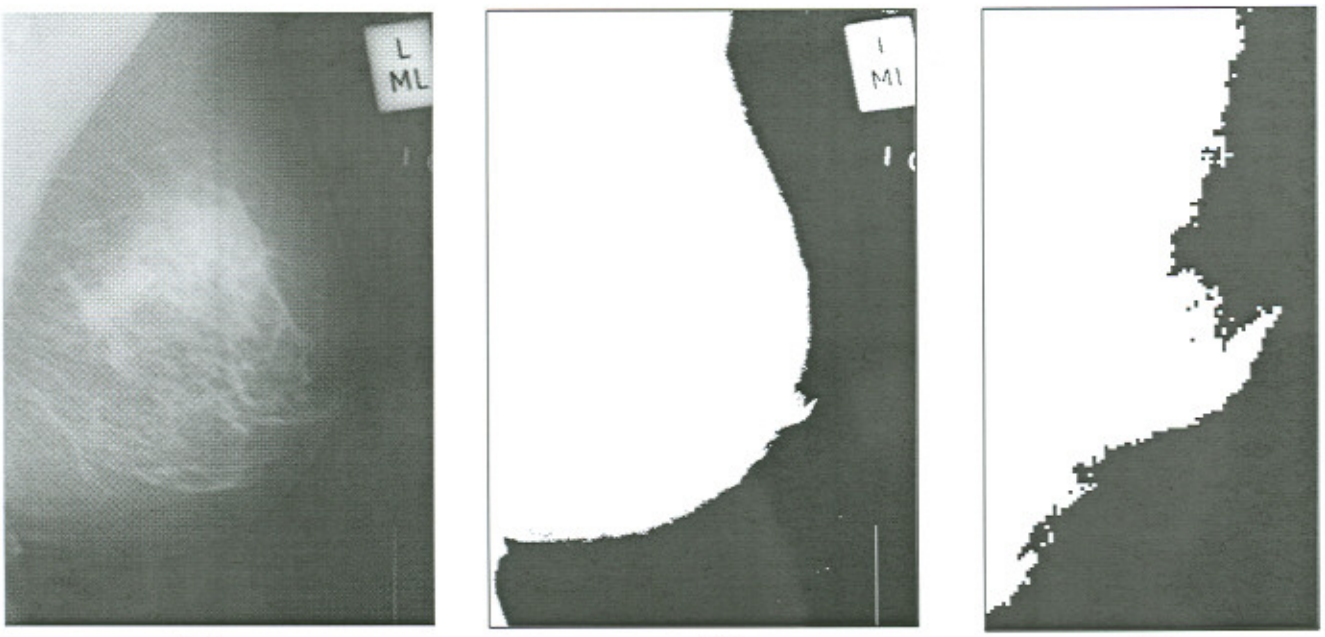

Fig.2

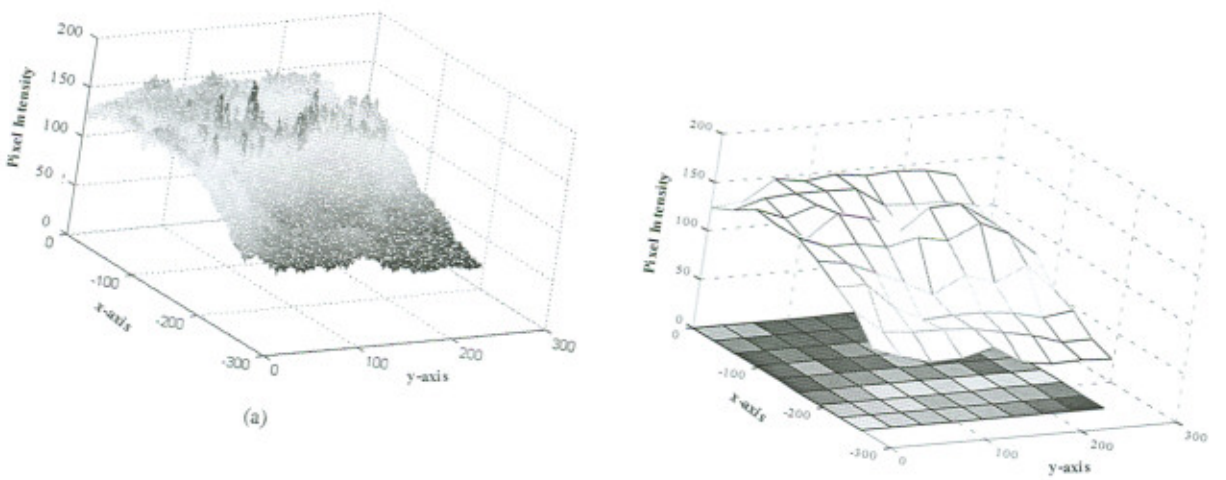
Pixel Intensity
200
150
100
50
0
0
-100
-200
-300
x-axis
0
100
200
300
y-axis
(a)
Pixel Intensity
200
150
100
50
0
0
-100
-200
-300
x-axis
0
100
200
300
y-axis
(b)

Fig.3

(a) (b) (c)

Fig. 4

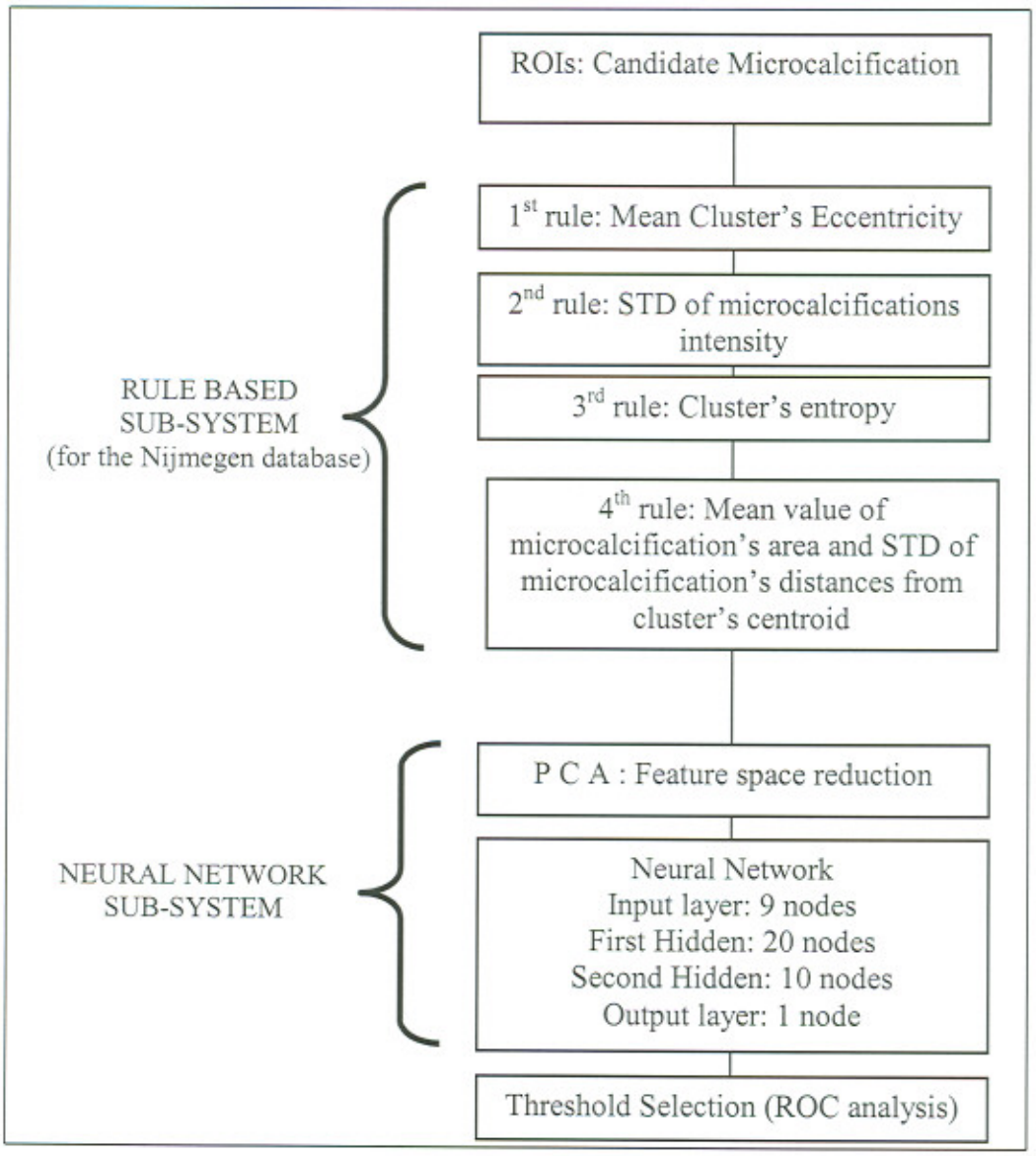
ROIs: Candidate Microcalcification
1st rule: Mean Cluster's Eccentricity
2nd rule: STD of microcalcifications intensity
3rd rule: Cluster's entropy
4th rule: Mean value of microcalcification's area and STD of microcalcification's distances from cluster's centroid
RULE BASED SUB-SYSTEM (for the Nijmegen database)
P C A : Feature space reduction
Neural Network
Input layer: 9 nodes
First Hidden: 20 nodes
Second Hidden: 10 nodes
Output layer: 1 node
NEURAL NETWORK SUB-SYSTEM
Threshold Selection (ROC analysis)

Fig. 5

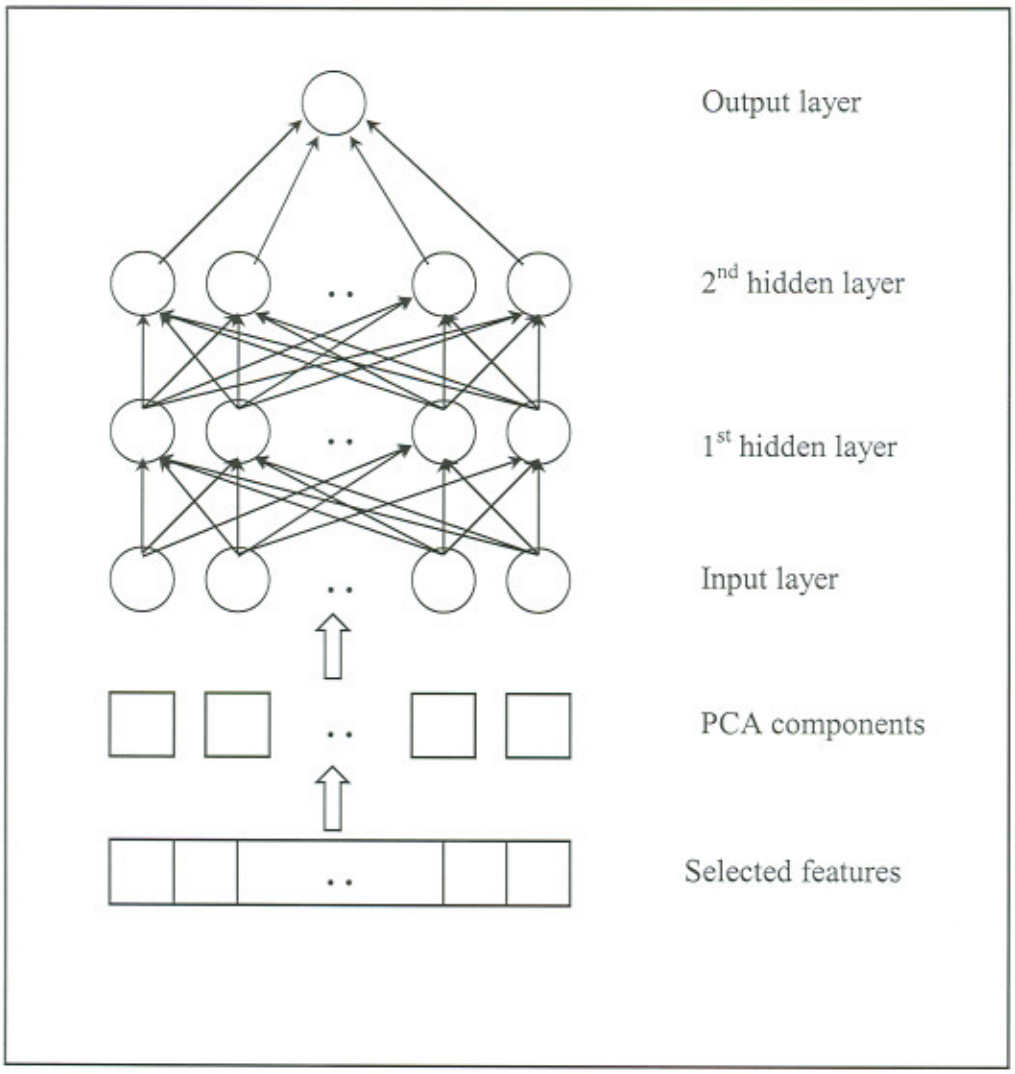
Output layer
2nd hidden layer
1st hidden layer
Input layer
PCA components
Selected features

Fig.6

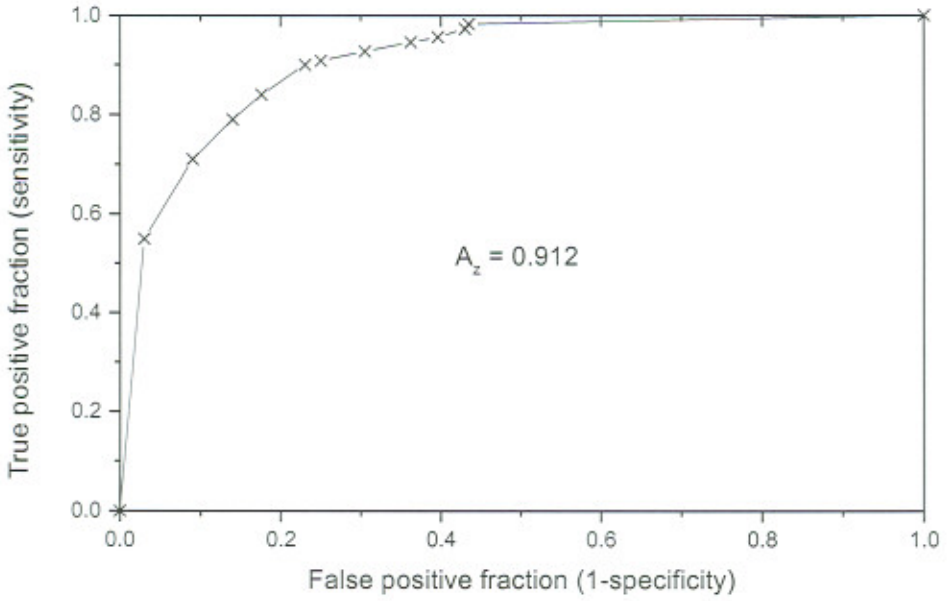
True positive fraction (sensitivity)
False positive fraction (1-specificity)
A_z = 0.912
0.0
0.2
0.4
0.6
0.8
1.0

Fig. 7

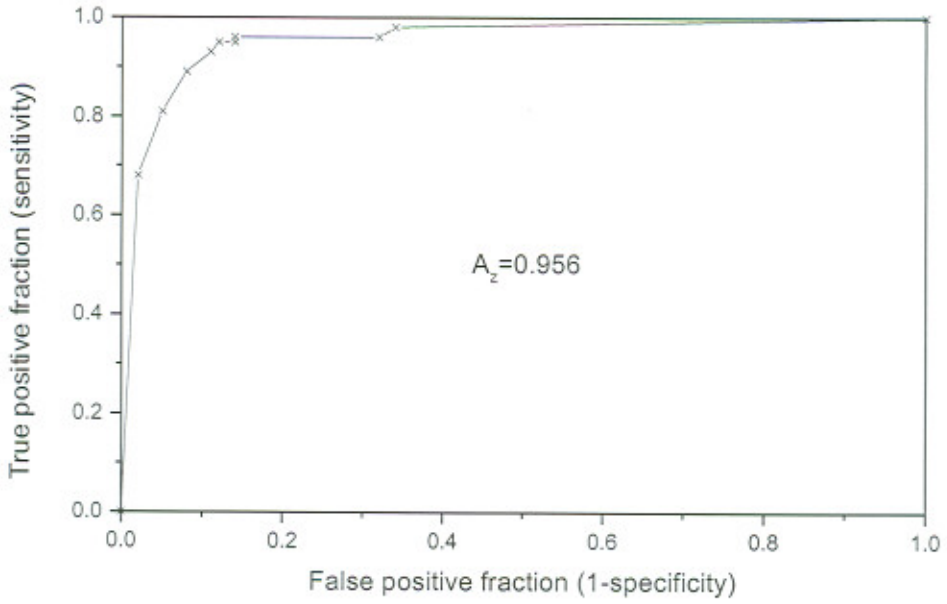
True positive fraction (sensitivity)
False positive fraction (1-specificity)
A_z=0.956
0.0
0.2
0.4
0.6
0.8
1.0

Fig. 8

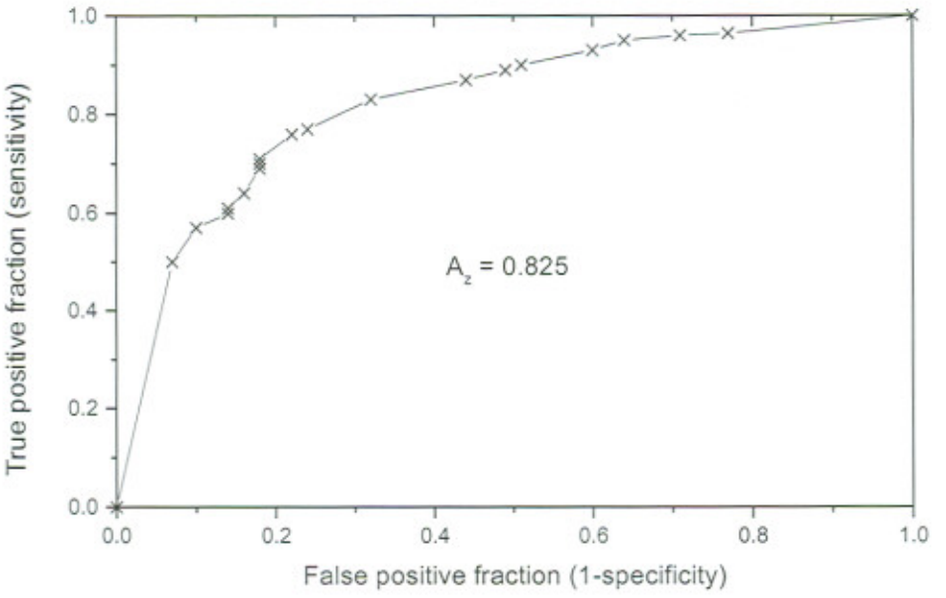
True positive fraction (sensitivity)
False positive fraction (1-specificity)
A_z = 0.825
0.0
0.2
0.4
0.6
0.8
1.0

Fig. 9

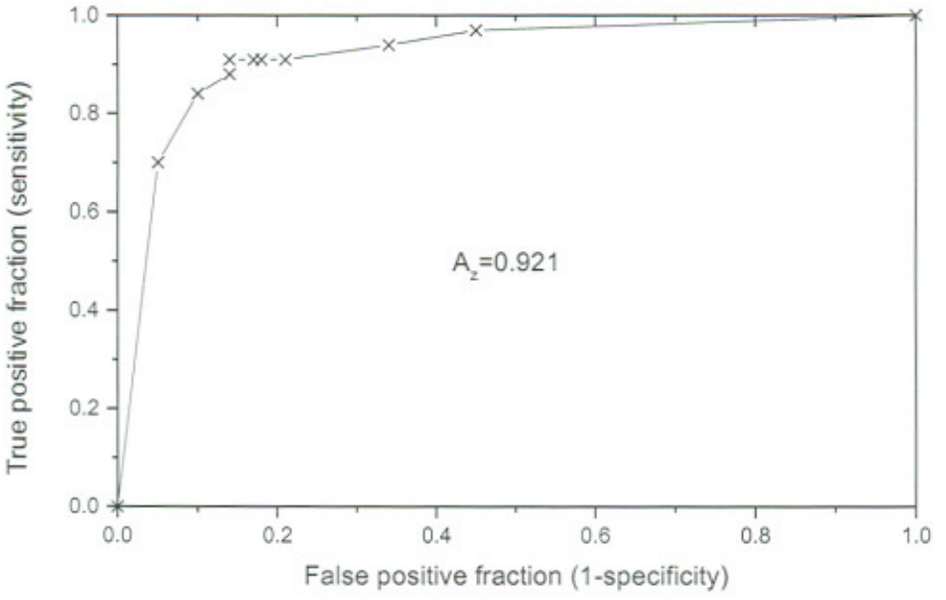
True positive fraction (sensitivity)
False positive fraction (1-specificity)
A_z=0.921
0.0
0.2
0.4
0.6
0.8
1.0

Fig. 10

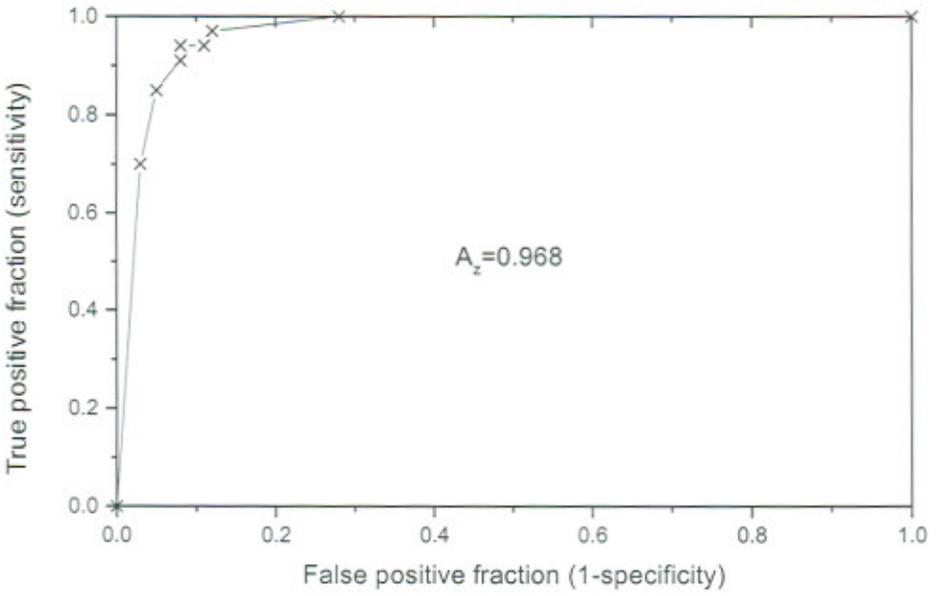
True positive fraction (sensitivity)
False positive fraction (1-specificity)
A_z=0.968
0.0
0.2
0.4
0.6
0.8
1.0

Fig. 11

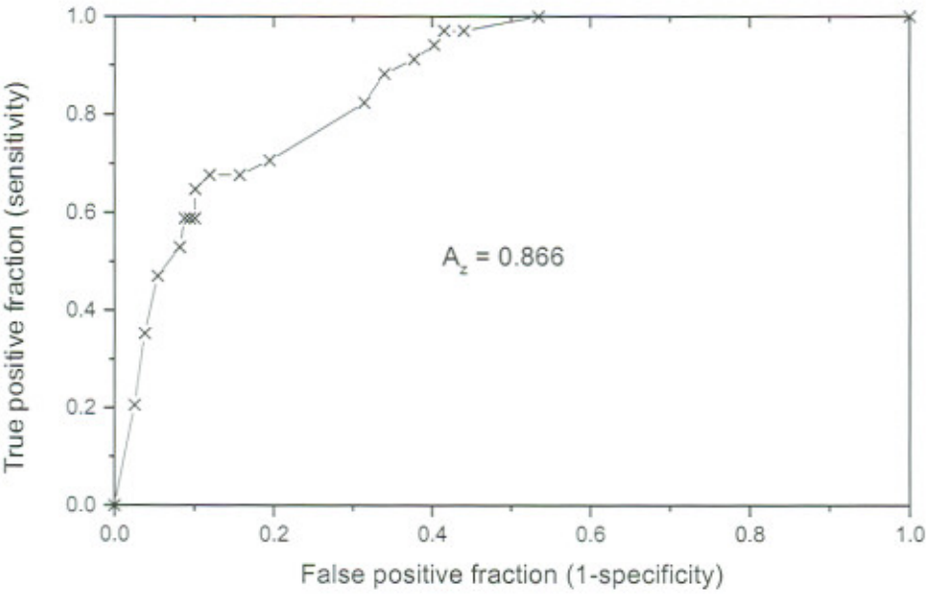
True positive fraction (sensitivity)
False positive fraction (1-specificity)
A_z = 0.866
0.0
0.2
0.4
0.6
0.8
1.0

Fig. 12

(Illustrations' captions)

Figure 1: The microcalcification cluster detection system.

Figure 2: (a) An original mammogram, (b) the different objects appearing in the binary image and (c) a zoom view in the area of the breast skinline.

Figure 3: (a) 3D intensity representation of a 300×300 pixel area, (b) calculated object's background intensity of the same area.

Figure 4: (a) A part of a mammogram (original image), (b) the output of the segmentation component and (c) the binary image after small object elimination.

Figure 5: The hybrid classification system.

Figure 6: The neural network sub-system.

Figure 7. ROC curve obtained with the hybrid intelligent system using the Nijmegen database with cross validation.

Figure 8. ROC curve obtained with the hybrid intelligent system using the Nijmegen database (complete set).

Figure9. ROC curve obtained with the neural network system using the Nijmegen database with cross validation.

Figure 10. ROC curve obtained with the hybrid intelligent system using the MIAS database with cross validation.

Figure 11. ROC curve obtained with the hybrid intelligent system using the MIAS database (complete set)..

Figure12. ROC curve obtained with the neural network system using the MIAS database with cross validation.